THE JOURNAL OF PHYSICAL CHEMISTRY B

Article

pubs.acs.org/JPCB

Incorporation of Ubiquinone in Supported Lipid Bilayers on ITO

Javier Hoyo,[†] Ester Guaus,[†] Gerard Oncins,[‡] Juan Torrent-Burgués,*[,†,§,∥] and Fausto Sanz[§,∥,⊥]

[†]Universitat Politècnica de Catalunya, Dpt. Enginyeria Química, 08222 Terrassa (Barcelona), Spain

[‡]Universitat de Barcelona, Centres Científics i Tecnològics (CCiTUB), 08028 Barcelona, Spain

[§]Institut de Bioenginyeria de Catalunya (IBEC), 08028 Barcelona, Spain

[∥]CIBER-BBN, Campus Rio Ebro-Edificio I+D, 50018 Zaragoza, Spain

[⊥]Universitat de Barcelona, Dpt. Química-Física, 08028 Barcelona, Spain

ABSTRACT: Ubiquinone (UQ) is one of the main electron and proton shuttle molecules in biological systems, and dipalmitoylphosphatidylcholine (DPPC) is one of the most used model lipids. Supported planar bilayers (SPBs) are extensively accepted as biological model membranes. In this study, SPBs have been deposited on ITO, which is a semiconductor with good electrical and optical features. Specifically, topographic atomic force microscopy (AFM) images and force curves have been performed on SPBs with several DPPC:UQ ratios to study the location and the interaction of UQ in the SPB. Additionally, cyclic voltammetry has been used to understand the electrochemical behavior of DPPC:UQ SPBs. Obtained results show that, in our case, UQ is placed in two main different positions in SPBs. First, between the DPPC hydrophobic chains, fact that originates a decrease in the breakthrough force of the bilayer, and the second between the two leaflets that form the SPBs. This second position occurs when increasing the UQ content, fact that eventually forms UQ aggregates at high concentrations. The formation of aggregates produces an expansion of the SPB average height and a bimodal distribution of the breakthrough force. The voltammetric response of UQ depends on its position on the bilayer.

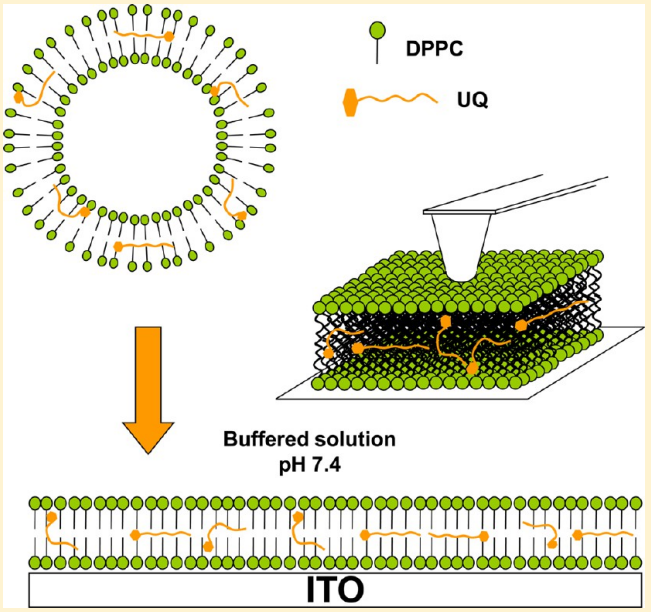

INTRODUCTION

Artificial lipid bilayers have been extensively studied as models that mimic natural membranes. They have shown their importance in a broad range of chemical and biological applications, with the development of artificial photoelectric devices being one of the most encouraging.[1−5] The main characteristic of lipid membranes is that they can self-organize and also interact with biomolecules, both within the membrane and at its surface, due to the phospholipids' amphiphilic character and electrostatic charge.[2,6]

A supported planar bilayer (SPB) consists of the deposition of a bilayer on a solid support, where only the upper surface is exposed to the solution. The high stability of these membranes, the possibility to work in both liquid or gel phases, the possibility to tune the composition, and the ability to be characterized with several techniques make SPBs a biological membrane model.[4,6−8]

SPB can be obtained mainly by two techniques, the Langmuir−Blodgett (LB) or LB+Langmuir Schafer method and the other the vesicle fusion technique, which can be performed directly on a naked solid substrate or on a precoated solid substrate.[2,6] This second technique involves vesicles which are closed shells dispersed in aqueous medium and that are able to trap inside other molecules.[2,9]

A good vesicle extension and fusion process is the key for achieving a high quality membrane with little defect density. To obtain this, the solid surface is of high relevance: It should be hydrophilic, smooth, and clean, so mica and silica are the most used.[6] Besides the solid surface, the extension and fusion mechanism also depends on vesicle size and method of preparation,[6,10] according to theoretical models.[11,12]

In addition to the correct bilayer spreading, SPB substrates must show other features depending on the applications, for instance, when a conductive substrate is needed. In this line, several attempts of SPBs have been performed on gold,[13,14] silver,[15,16] platinum,[17] and indium tin oxide (ITO).[3,6,18,19] ITO

Received: January 15, 2013
Revised: April 26, 2013

   dx.doi.org/10.1021/jp4004517 | J. Phys. Chem. B XXXX, XXX, XXX−XXX

Scheme 1. (A) Ubiquinone-10, (B) Plastoquinone-9, (C) Dipalmitoylphosphatidylcholine

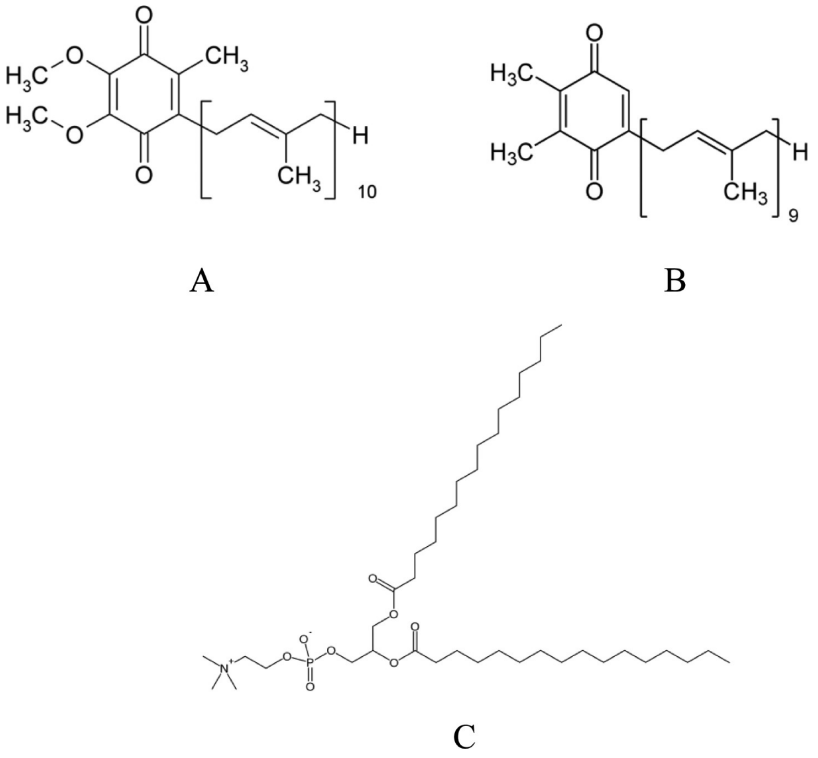

is a hydrophilic semiconductor with relatively high conductivity and good optical features,[20] which makes it a good candidate for artificial photosynthesis studies. In order to investigate this, several attempts have been performed to extend SPBs on ITO surface. This is the case of SPBs deposited by vesicle fusion on ITO.[1,18,19] Yang and Kleijn[21] used the LB technique to prepare SPB on hydrophilic and hydrophobized ITO, and Devados[22] prepared the SPB by sonication of the ITO in an ethanol solution containing the phospholipid. The preparation of a cushion layer on the ITO surface previously to the SPB extension has been revealed as a good solution for decreasing the effect of the ITO roughness. Using this method, Hillebrandt et al.[23] deposited a polymer film on the ITO surface, achieving a higher electrical resistance than without the polymer film, and McBee et al.[24] used also a conductive polymer film to study the proton transport across the SPB.

AFM is a suitable technique for imaging SPBs because it can obtain high resolution images in a liquid environment.[7,25] Force spectroscopy can also be used to perform controlled force–distance curves on the SPB and to obtain information about the interaction between the AFM probe and the sample surface. This way, SPB mechanical properties and other features like height estimation, van der Waals forces, electrostatic forces, and solvation and hydration forces can be characterized.[25−27] AFM and other force spectroscopic techniques have been performed on SPBs using several substrates like SiO_2, highly oriented pyrolitic graphite (HOPG), and mica,[26] with this last substrate being one of the most used because of its atomically flat surface and cleanliness once freshly cleaved.

The electrochemical response of SPBs on ITO has been evaluated by impedance spectroscopy[1,18,19,23] and voltammetry.[1,21,22] These works were focused on checking the bilayer compactness and stability, but only refs 1 and 24 used SPBs to study the electrochemical behavior of a confined species.

Ubiquinone-10 (UQ) (Scheme 1A) and plastoquinone-9 (PQ) (Scheme 1B) are involved in bioenergetic processes acting as electron and proton shuttles in mitochondrial and thylakoid membranes, respectively.[28] The structure of these molecules consists of a quinonic ring acting as a redox center and a long isoprenoid chain which confers a high hydrophobic character to the molecule. Several works have studied the use of different quinonic molecules instead of using PQ for electron and proton exchange in artificial photosynthesis studies,[29−32] and Hoyo et al.[33] showed that UQ is a good candidate for substituting PQ in these studies.

In the present work, we study the incorporation of UQ in vesicles of the model phospholipid dipalmitoylphospatidylcholine (DPPC) and use ITO as a substrate for obtaining the corresponding SPBs. The resulting SPBs are characterized topographically using liquid-AFM and mechanically with the aid of controlled force curves. Moreover, the redox behavior of the confined UQ molecules is evaluated using cyclic voltammetry and is compared with that obtained for a DPPC:UQ monolayer transferred on ITO by the Langmuir–Blodgett technique.[32] Here, we present, at the best of our knowledge, the first force spectroscopy study of SPB deposited on ITO, thanks to the low roughness of the used ITO and the SPB preparation method. The inclusion of UQ in SPB on such a substrate represents a step forward in applications of biomimetic membranes.

EXPERIMENTAL SECTION

Materials. Dipalmitoylphospatidylcholine (DPPC) was purchased from Avanti Polar Lipids, and ubiquinone-10 (UQ) HPLC grade was from Sigma-Aldrich. KH_2PO_4, KCl, and chloroform of analytical grade were used in solution preparation. Water was ultrapure Milli-Q (18.2 MΩ·cm).

dx.doi.org/10.1021/jp4004517 | J. Phys. Chem. B XXXX, XXX, XXX−XXX

Indium tin oxide (ITO) deposited on glass slides was purchased from SOLEMS (France).

Vesicle Formation. 3 mM pure component solutions were prepared in glass vials dissolving DPPC and UQ in chloroform. Samples were prepared mixing the appropriate volume of each pure component solution to achieve the desired DPPC:UQ molar ratio. The solutions were dried under slow argon flow, and lipids were resuspended by adding 2 mL of buffer solution (0.150 M KCl as supporting electrolyte at pH 7.4 adjusted with the KH_2PO_4/K_2HPO_4 buffer). Six cycles of 50 s of vortexing−heating (60 °C) followed by 30 min of sonicating (60 °C) were performed to obtain unilamellar vesicles. These solutions were kept at 4 °C during a maximum of 3 weeks.

SPB Formation. Vesicle solution was sonicated 30 min at 60 °C and then added inside an O-Ring placed on the ITO slide surface that had been previously cleaned once with ethanol and three times with Milli-Q grade water. After the vesicle deposition, the ITO slides were placed in an oven for 40 min using a homemade environmental cell which maintains a high moisture level, permitting to achieve 85 °C without drying the sample. After this incubation process, the ITO surface was washed three times using the buffer solution. The resulting SPB was kept wet, using the buffer solution, before and during the experiments to preserve its integrity.

AFM Characterization. AFM topographic images of the SPBs were acquired in liquid tapping mode using a Multimode AFM controlled by a Nanoscope IV electronics (Bruker, Santa Barbara, CA). Triangular AFM probes with silicon nitride cantilevers and silicon tips were used (SNL-10, Bruker). Their nominal spring constant was 0.35 $N{\cdot}m^{-1}$. Images were acquired at 1.5 Hz and at minimum vertical force so as to reduce sample damage. AFM images were obtained from at least two different samples, prepared on different days and by scanning several macroscopically separated areas on each sample.

SPB thickness was determined using the following method: After acquiring a topographic image where ITO exposed areas and SPBs were present, height histograms of the pixels corresponding to the top of the SPBs and ITO regions were compared. Then, the height difference between the two peaks of the histogram was calculated and presented as reported SPB height values.

Force Curves. The same probes were used for topographic and force measurements. Quantitative force measurements were carried out by calibrating each AFM probe individually so as to experimentally find their spring constant, k. To do that, probe sensitivity ($V{\cdot}nm^{-1}$) was measured by performing force curves on a hard substrate (silicon oxide), a process which was immediately followed by the thermal noise calculation,[34] which calculates the k value by fitting the shape of the resonance peak obtained without external probe excitation. After this process, the laser position on the cantilever surface and the photodetector position remained unchanged to ensure that calibration parameters remained constant during the experiment on SPBs. Force curves were performed at a constant rate of 1 Hz, and only one indentation was performed in every position so as to measure the nanomechanical properties of fresh sample regions in every individual experiment. Sets of at least 300 force curves over different places of the sample were acquired from at least two different samples with different tips to ensure reproducibility.

Electrochemical Characterization. The voltammetric measurements were performed in a conventional three-electrode cell using an Autolab Potentiostat-Galvanostat PGSTAT-12 (Ecochemie, NL). Working electrodes were freshly cleaned ITO slides (10 mm × 25 mm) covered with the SPBs. The counter electrode was a platinum wire in spiral geometry, and the reference electrode was an Ag/AgCl/3 M KCl microelectrode (DRIREF-2SH, World Precision Instruments). This reference electrode was mounted in a Lugging capillary containing KCl solution at the same cell concentration. All reported potentials were referred to this electrode. The electrochemical cell contained 0.150 M KCl as supporting electrolyte at pH 7.4 adjusted with the KH_2PO_4/K_2HPO_4 buffer solution. All solutions were freshly prepared with Milli-Q grade water and deaerated with a flow of Ar gas for 15 min prior to cyclic voltammetry (CV) experiments, which were conducted at 22 ± 1 °C. Voltammetric experiments were carried out at different scan rates, scanning toward negative potentials in a homemade glass cell with a reaction area of 33 mm^2.

RESULTS AND DISCUSSION

In this section, using AFM and force curves, the topography and mechanical properties of DPPC and DPPC:UQ samples are studied so as to correlate the different behavior of SPBs on ITO referred to bare ITO. SPB are also characterized using cyclic voltammetry in order to obtain the electrochemical response of the inserted UQ.

Topography. Figure 1 corresponds to an AFM image of bare ITO. This image shows large flat areas with rounded

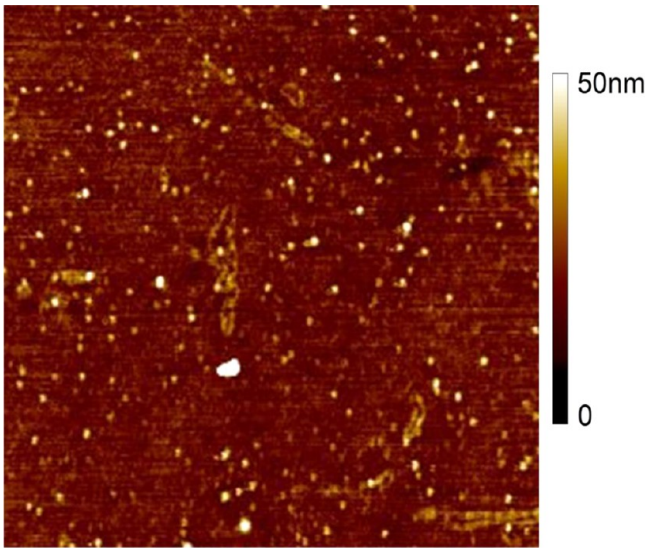

Figure 1. Topographic AFM image (5 μm × 5 μm) of bare ITO.

structures corresponding to nanometric inhomogeneities for the ITO film. The mean roughness of this commercial ITO is 1.2 ± 0.6 nm, with this value being slightly lower than the values of 1.4−2 nm observed by previous authors.[3,21] This low surface roughness permits the formation and observation of larger SPB islands.

Figure 2 depicts the AFM images of SPBs of DPPC and DPPC:UQ 5:1 mixture, respectively. AFM images of DPPC:UQ 10:1 and 20:1 mixtures show a similar appearance to that of DPPC:UQ 5:1. These images confirm that the SPB is formed on ITO. The images presented in Figure 2 show two main zones corresponding to two different materials, confirmed both topographically and by the respective contrast phase

dx.doi.org/10.1021/jp4004517 | J. Phys. Chem. B XXXX, XXX, XXX−XXX

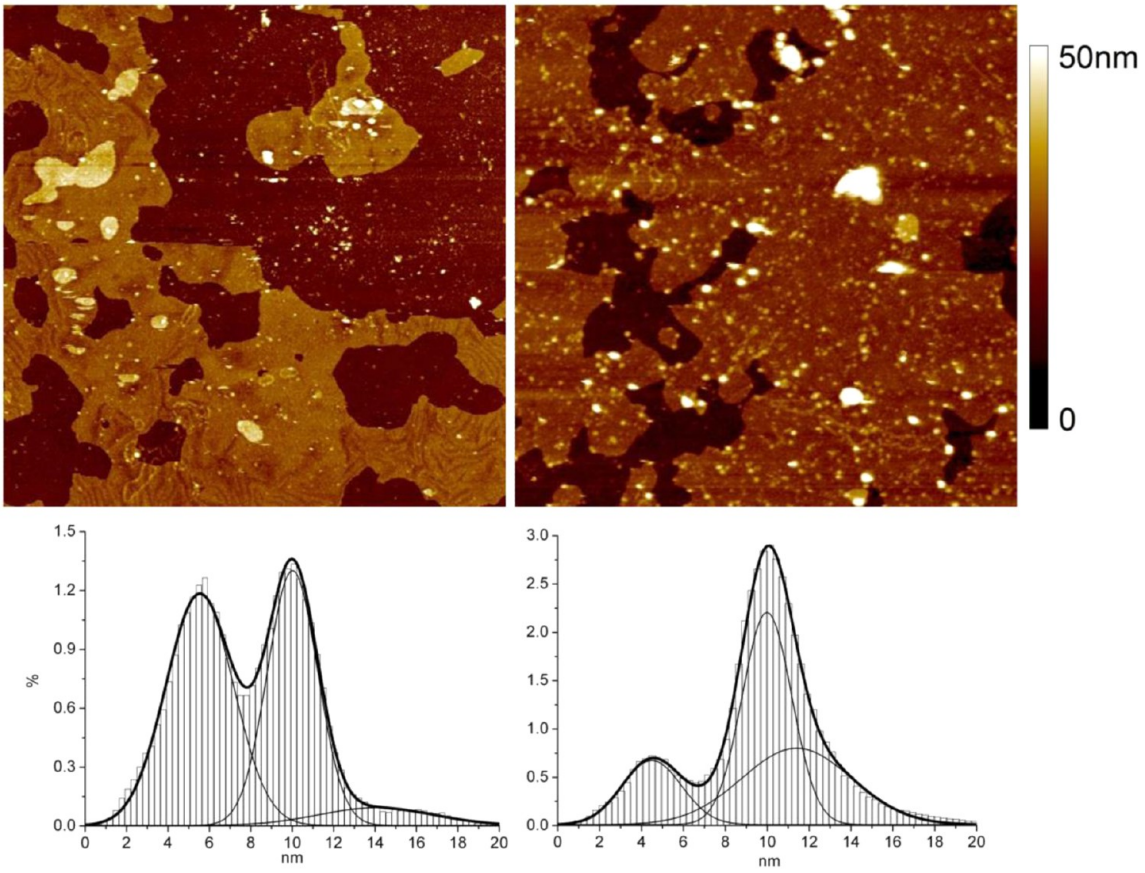

Figure 2. Topographic AFM images (5 μm × 5 μm) of SPB of DPPC (left) and DPPC:UQ 5:1 (right), and height distributions (columns) using a slim line for fitted peaks and a thick line for the peak convolution. The SPB height respect to ITO surface was calculated from the distance between distribution peaks. Images were acquired in liquid tapping mode.

images (not shown). Dark zones correspond to a naked ITO surface, which is taken as zero level for further studies, and fair zones correspond to SPB islands.

The SPBs shown in this work represent a surface coating from 50 to 70%, being lower than the 89% achieved on mica,[25] which is an atomically flat substrate with sub-nanometric roughness. This difference can also be due to the interfacial chemistry, since both substrates are different. Patches of multilayers corresponding to the spreading of non-unilamellar vesicles are rarely seen.

The topographic images permit one to quantify the average height of the SPBs, as explained in the Experimental Section. This height is measured to be 4.6 ± 0.3 nm for all the studied compositions except for DPPC:UQ 5:1, which presents a height of 5.7 ± 0.3 nm, indicating an expansion of the bilayer. A more accurate analysis of the height distribution (see Figure 2) shows a deconvolution in two peaks for the DPPC:UQ 5:1, centered at 5.5 ± 0.3 and 6.9 ± 0.3 nm, the latter with lower frequencies. It can be inferred that the pure DPPC bilayer spread on ITO has a similar thickness as the pure DPPC SPBs spread on mica, 4.7 ± 0.2[35] or 4.8 ± 0.3 nm,[25] but slightly lower than the values of 5.7 ± 0.3[36] and 5.5 ± 0.1 nm[37,38] obtained by other authors. Molecular dynamic simulations[39] provide a value of 4.2 nm for the DPPC bilayer, in more accordance with our value. The higher reported values can be attributed to the presence of a thin layer of water between the ITO surface and the bilayer.[2,6,7,36] The second peak in the pure DPPC height distribution of Figure 2, which presents low frequencies, corresponds to a double SPB, in concordance with the patches observed in the topographic image. Nussio et al.[35] also studied the pure DPPC SPB's height on several hydrophilic substrates with different roughness. The results obtained by Nussio et al. are in agreement with our experimental observations, indicating that the substrate roughness has no significant influence in the bilayer height. Another observation is that the insertion of UQ in the DPPC SPB has no influence on the average height for low UQ concentrations, indicating that these molecules mainly embed and distribute uniformly between the DPPC matrix. At higher UQ concentrations (5:1), these molecules cannot be correctly distributed so they may form pools or aggregates of UQ[40] that locally expand the bilayer thickness. This fact is commented on in the next section in correspondence with the force curve results.

Force Curves. Force spectroscopy characterization of samples was performed using force−extension curves, which provide information on the interaction forces between neighboring molecules and on the mechanical properties of the SPB. Force−extension curves were performed on the central regions of SPBs to avoid rim effects.

The threshold force (*Fy*) is the force at which the SPB locally collapses due to the vertical force exerted by the AFM tip. In fact, it can be regarded as a fingerprint of a certain sample, as demonstrated in a previous work.[35] Conceptually, *Fy* marks the transition between the elastic regime and the plastic deformation or fragile rupture. Because of that, *Fy* gives an accurate idea of the intermolecular interaction forces that arise inside the SPB and also of the possible electrostatic interactions that bind SPBs to substrates. In our case, experimental *Fy*

dx.doi.org/10.1021/jp4004517 | J. Phys. Chem. B XXXX, XXX, XXX−XXX

values are used to assess molecular rearrangements when preparing DPPC SPBs with different UQ ratios at a selected temperature and buffer conditions.

Figure 3A shows the basic scheme of an AFM working on the force spectroscopy mode. In each force curve, the cantilever deflection, which is proportional to the vertical force exerted on the sample, is 0 before the tip−sample contact (point 1, Figure 3B). Increasing the tip compression on the SPB, the vertical force increases until the layer breaks due to the pressure exerted on it. This breakthrough appears as a sudden jump in the force curve (point 2, Figure 3B), with this value being the *Fy* measurement. As the vertical force keeps on increasing, the tip is in contact with the sample substrate. A more handy representation of the force curve (vertical piezo displacement vs vertical force) is the penetration curve (FvP), that is, sample penetration depth vs vertical force. The inset of Figure 3B shows this kind of representation, where two characteristic regions can be easily recognized; from point 1 to 2, the curve shows the elastic compression of the sample. At higher forces (after the breakthrough event), the plastic compression of the substrate is represented. Interestingly, the elastic region of the FvP comprises two different interactions. First of all, electrostatic forces between tip and sample, which arise when the electrical double layer induced by the zwitterionic headgroups of DPPC meets the slightly negative charge of the AFM tip. This force was measured to be extremely small for similar AFM probes under these conditions of ionic strength and pH,[8] so its effects will be neglected in the analysis of the data. Second, the mechanical deformation of the sample, which will be considered to account for the totality of the measured interaction.

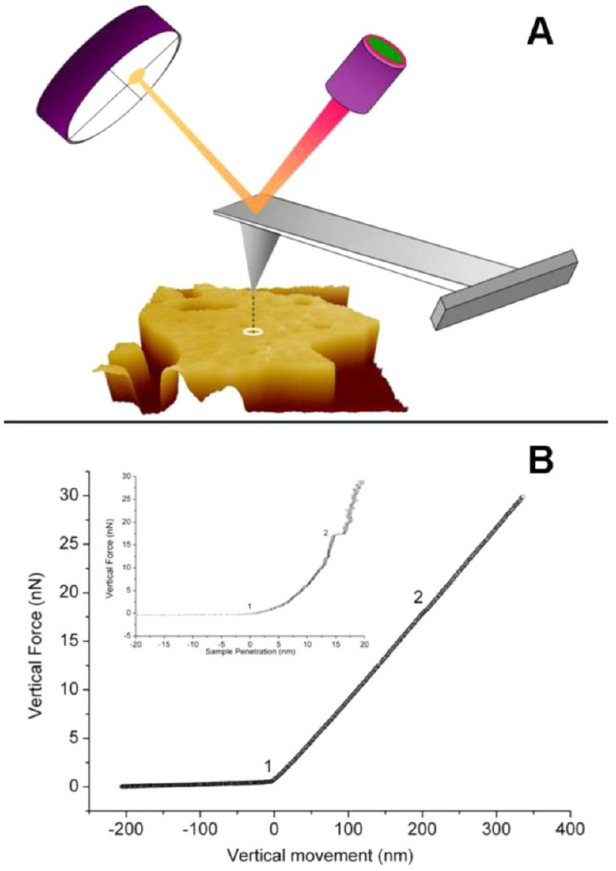

Figure 3. (A) AFM tip−sample scheme when executing a force curve. (B) Characteristic force curve for a DPPC:UQ 5:1 mixture (inset: FvP of a characteristic force curve for a DPPC:UQ 5:1 mixture).

Figure 4 shows histograms corresponding to *Fy* values obtained from individual FvP curves for different compositions of SPBs. For the sake of simplicity, the data has been fitted using a Gaussian model, although the continuum nucleation model proposed by Butt et al. could also be used.[41,42] The obtained results are 32.8 ± 7.1 nN for pure DPPC, 24.0 ± 6.6 nN for DPPC:UQ 20:1, and 20.8 ± 5.6 nN for DPPC:UQ 10:1. DPPC:UQ 5:1 presents a bimodal distribution, with the first mode centered at 15.2 ± 6.0 nN and the second at 38.7 ± 5.7 nN. It can be clearly seen that the *Fy* value decreases when the UQ content in the SPB increases. This fact can be explained by the increase of the area per molecule caused by the insertion of UQ in the DPPC matrix, which causes a weakening of lateral alkyl−alkyl interactions, producing a decrease in the compactness of the layer. In previous works, *Fy* values, measured on a DPPC SPB on mica and under similar ionic strength and pH buffer conditions, presented a mean value of 28.6,[35] 25,[27] or 21.4 nN,[8] being lower than the value of 32.8 nN determined by us on ITO. ITO and mica are hydrophilic substrates with similar isoelectric points, so these small differences can be explained mainly by the different chemical compositions of the surface and, secondly, by the different cations present in the buffer, as seen by Redondo-Morata et al.[8] who observed a 7 nN

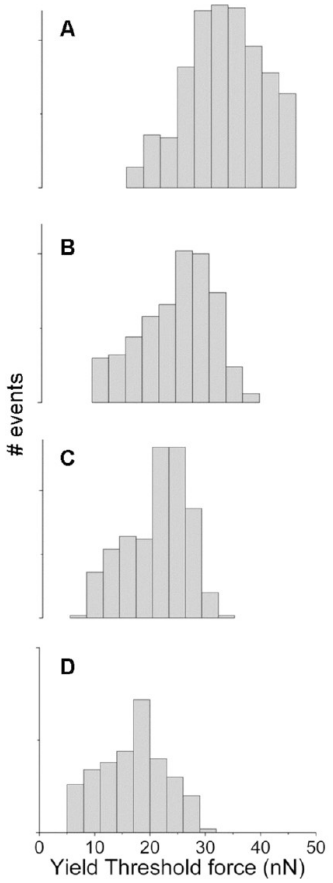

Figure 4. Yield threshold histograms obtained from force curves on SPBs of DPPC (A), DPPC:UQ 20:1 (B), DPPC:UQ 10:1 (C), and DPPC:UQ 5:1 (D).

dx.doi.org/10.1021/jp4004517 | J. Phys. Chem. B XXXX, XXX, XXX−XXX

increase of the *Fy* value for DPPC SPBs on mica when Na^+ was exchanged by K^+ in the buffer.

The existence of a bimodal distribution for the DPPC:UQ 5:1 system is explained by the formation of UQ pools or aggregates when the UQ concentration is high. These pools provoke bilayer local expansions, as has been explained in the previous section where two heights are observed in the AFM images. The indentation in these expanded zones, with higher height, is more difficult than that in the standard zones, so a higher *Fy* is required. Thus, the presence of standard (15.2 ± 6.0 nN) and expanded zones (38.7 ± 5.7 nN) leads to each mode of the histogram.

Electrochemical Characterization. The electrochemical behavior of bare ITO electrode, ITO/DPPC SPB, and ITO/DPPC:UQ SPB has been studied by cyclic voltammetry in the electrolyte solution at pH 7.4. A bare ITO electrode (not shown) presents no REDOX response in the working screen placed between 1 and −0.7 V. From the voltammograms, we can estimate the value of the interface capacitance (C_d) that is around 1 $\mu F \cdot cm^{-2}$. The ITO/DPPC bilayer presents C_d values between 3 and 4 $\mu F \cdot cm^{-2}$ for the potential screen compressed between 1 and −0.2 V, indicating that the ITO/DPPC bilayer system is more accessible to the electrolyte ions than the bare ITO electrode surface, and that the lipid bilayer presents few defects.[43−45] At more cathodic potentials than −0.2 V, a continuous increasing of the current values is obtained for the ITO/DPPC bilayer, indicating that the hydrogen evolution becomes important. The capacitance values are in accordance with that obtained for an ITO/DPPC monolayer extracted by the Langmuir−Blodgett technique,[32] although in this case hydrogen evolution starts at −0.4 V at a surface pressure of 40 $mN \cdot m^{-1}$. The fact that the hydrogen evolution starts at more positive potentials in the case of the vesicle fusion SPB system can be attributed to a lower order and uniformity in the bilayer obtained by this technique.[46] Studies of the effect of electrical potential on lipid supported bilayers[18,21,44−46] show that, imposing a progressively more negative potential at the electrode surface, the bilayer becomes less ordered, apparently swells, and finally is detached from the electrode surface. In this reversible process, the bilayer remains near the surface only separated by a layer of electrolyte.

Figure 5 shows the cyclic voltammetric response of the ITO/DPPC:UQ system using the buffered electrolyte solution, scanning toward negative potentials. The gray dotted line corresponds to the response of pure DPPC (blank experiment). It shows a good baseline in the working screen. The black solid line corresponds to the system DPPC:UQ 5:1 presenting one main peak for reduction and two peaks for oxidation. The DPPC:UQ 10:1 system (black dotted line) presents a similar behavior but having a peak intensity quite shorter than 5:1. DPPC:UQ 20:1 (solid gray line) presents a wave without appreciable intensity peaks, having a cyclic voltammetric response close to the pure DPPC. In this last case, the electrochemical response is similar to that obtained for adsorbed vesicles of liposomes containing UQ.[47]

We label oxidation peaks as I_O and II_O, respectively. The inset of Figure 5 presents the cyclic voltammetric response of the DPPC:UQ system on ITO in a shorter potential screen than Figure 5. Comparing both figures, an increase in the current intensity of peak II_O can be seen when scanning to more negative potentials. This observation confirms that the reduction peak is a convolution of two processes, I and II. The UQ reduction via process I is better seen at low UQ content

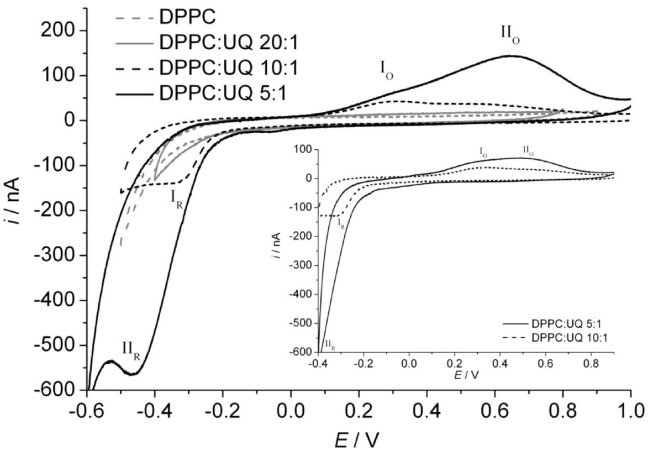

Figure 5. Cyclic voltammograms of DPPC and DPPC:UQ mixture SPBs using the buffered solution at 23 ± 1 °C. Inset: Voltammograms for the same systems but with a shorter potential screen.

(see peak I_R in Figure 5), whereas at high UQ content the reduction via process II becomes more important, masking peak I_R. The inset also confirms that process I is more reversible than process II.

The formal reduction potential of processes I and II referred to the Ag/AgCl/KCl (3 M) reference electrode can be calculated, and the values $E_f(I) = -0.010 \pm 0.020$ V for process I and $E_f(II) = 0.09 \pm 0.020$ V for process II have been obtained. These values are very close to those obtained by Hoyo et al.[32] for ITO/DPPC:UQ monolayers.

Further information of the ITO/DPPC:UQ electrochemical system can be obtained using cyclic voltammetry at different scan rates. Discarding the DPPC:UQ 20:1 system because no REDOX response was obtained, both 5:1 and 10:1 systems present a good linear dependence between the scan rate and the peak current intensity (Figure 6). The linear dependence indicates that UQ molecules are surface confined[48] and the electrochemical process is not diffusion controlled.

The overall reaction of charge transfer for the redox couple UQ/UQH_2 can be described as

$$UQ + 2e + 2H^+ \leftrightarrows UQH_2$$

The E_f values obtained in this work for the ITO/DPPC:UQ bilayer system and those obtained for the ITO/DPPC:UQ

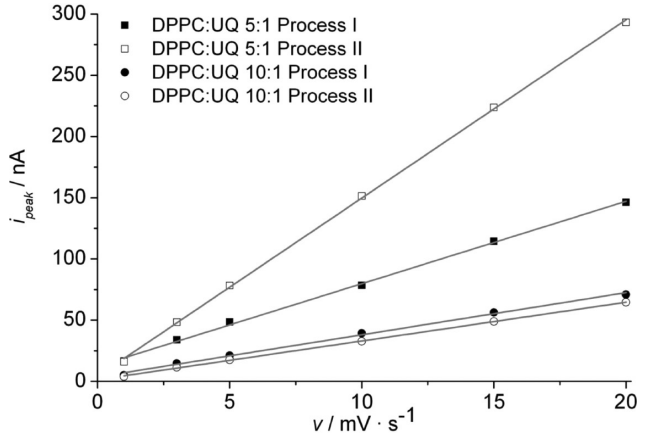

Figure 6. Oxidation peak intensity dependence vs scan rate for SPBs of DPPC:UQ 5:1 and 10:1.

dx.doi.org/10.1021/jp4004517 | J. Phys. Chem. B XXXX, XXX, XXX−XXX

monolayer system[32] are closer to the benzoquinone/hydroquinone system in aqueous solution than in an aprotic solvent, a fact that indicates that UQ molecules have H^+ ions available. This observation is also corroborated by Figure 6 where no diffusion dependence is obtained for the electrochemical process.

From these results and the studies of the electrical properties of SPB,[18,46] the ITO/DPPC:UQ system can be described as a two-component fluid supported membrane where the DPPC molecules act as electroinactive solvent and form a stable bilayer. The transport of ions through this bilayer was attributed to the ion diffusion in the hydrocarbon region after entrapment, thus following the Nagle and Scott's ion permeability theory. The diffusive movement is not the permeation-limiting process, but the ion entrapment is. This entrapment is produced by lateral density fluctuations that open short-lived cavities in the headgroup region of the bilayers into which ions can enter.[18]

The UQ molecules are embedded in the lipid matrix, and located at different positions according with the situations exposed by Hoyo et al.[32] Process I corresponds to the UQ/UQH_2 REDOX process for UQ molecules close to the ITO surface, and then inserted mainly in the bottom leaflet of the lipid bilayer. Process II correlates with the REDOX response for the UQ molecules lying at a higher distance of the electrode surface well in the midplane of the SPB or in the upper leaflet of the lipid bilayer. As can be seen in Figure 5, when increasing the UQ content, process II become more important, with the midplane being the main position at high UQ content.[40] These UQ clusters produce local expansions in the lipid bilayer, as has been explained in previous sections. Scanning toward negative potentials, the proton permeability of the SPB starts at more positive potentials than in the monolayers studied by Hoyo et al.[32] In the reduction process, this higher permeability produces the competition between the hydrogen evolution process and the UQ reduction at less negative potentials. The consequence of this earlier competition is the impossibility to deconvolute the reduction process into its three components: hydrogen evolution, I_R, and II_R.

The charge involved in the oxidation peak of the DPPC:UQ 5:1 system is 4.5 μC, being more than 2 times larger than that involved in DPPC:UQ 10:1 (1.8 μC). This result is in concordance with that obtained for a DPPC:UQ monolayer[32] and implies that the electroactive fraction increases with the UQ quantity in the bilayer. This behavior could be attributed to an electron hopping mechanism between UQ molecules in the electron transfer process that is favored at high densities of UQ in the bilayer.[49] From the oxidation charge, the surface coverage of UQ in the bilayer can be calculated, obtaining values of 70×10^{-12} and 27×10^{-12} mol·cm^{-2} for DPPC:UQ 5:1 and DPPC:UQ 10:1, respectively. The surface coverage for the DPPC:UQ 5:1 system, 70×10^{-12} mol·cm^{-2}, is higher than the expected value, 21×10^{-12} mol·cm^{-2}, calculated according to the mean area per molecule occupied by UQ[32] at the equivalent surface pressure of 30 mN/m for biological membranes.[50] This can be explained by the formation of UQ pools at the highest UQ concentration. On the other hand, this value is comparable with the value of 55.8×10^{-12} mol·cm^{-2} obtained at high surface pressure for a DPPC:UQ 5:1 monolayer.[32] When the UQ concentration is lowered, the surface coverage obtained for the DPPC:UQ 10:1 system, 27×10^{-12} mol·cm^{-2}, is closer to the expected value of 21×10^{-12} mol·cm^{-2} indicated for biological membranes.

CONCLUSIONS

DPPC:UQ SPBs were deposited on ITO, a transparent and conducting material. AFM images show no topographically significant visual differences depending on the DPPC:UQ ratio, but the SPB height increases for the 5:1 DPPC:UQ ratio, a fact that can be explained by the formation of UQ aggregates in the bilayer.

Force curves performed on top of the SPBs reveal a decrease of breakthrough force values when increasing the UQ content in the mixture, with this behavior being due to the weakening of the phospholipid intermolecular forces when UQ is added. DPPC:UQ 5:1 shows a bimodal distribution explained by the two structures detected topographically. First, zones of DPPC:UQ leaflets with UQ molecules uniformly distributed, and second, DPPC:UQ leaflets with UQ aggregations between the leaflets.

Cyclic voltammetry shows two differentiated processes: the first one corresponds to the REDOX behavior of the UQ molecules placed between the DPPC chains, and the second one corresponds to the UQ molecules placed in the SPB midplane. The latter process becomes more important when increasing the UQ content, which is in accordance with the UQ saturation in the DPPC matrix and its expulsion to the SPB midplane.

Obtained results also show that the employed technique is suitable for SPB formation on non-atomically flat hydrophilic substrates, as ITO, a fact that opens up prospect for artificial photosynthesis studies.

AUTHOR INFORMATION

Corresponding Author

*E-mail: juan.torrent@upc.edu. Phone: +34937398043. Fax: +34937398225.

Notes

The authors declare no competing financial interest.

ACKNOWLEDGMENTS

The authors acknowledge the economical support of the Spanish Government, through the Project CTQ2007-68101-C02, and of the Catalonia Autonomic Government, through the Project SGR2009-277. J.H. thanks Universitat Politècnica de Catalunya for the PhD grant.

REFERENCES

(1) Gao, H.; Luo, G. A.; Feng, J.; Ottova, A. L.; Tien, H. T. Fabrication and Photoelectric Properties of Self-Assembled Bilayer Lipid Membranes on Conducting Glass. *J. Photochem. Photobiol., B* **2000**, *59*, 87−91.

(2) Berti, D.; Caminatia, G.; Baglioni, P. Functional Liposomes and Supported Lipid Bilayers: Towards the Complexity of Biological Archetypes. *Phys. Chem. Chem. Phys.* **2011**, *13*, 8769−8782.

(3) Ge, C.; Orosz, K. S.; Armstrong, N. R.; Saavedra, S. S. Poly(aniline) Nanowires in Sol-Gel Coated ITO: a pH-Responsive Substrate for Planar Supported Lipid Bilayers. *ACS Appl. Mater Interfaces* **2011**, *7*, 2677−2685.

(4) Zhan, W.; Jiang, K. A Modular Photocurrent Generation System Based on Phospholipid-Assembled Fullerenes. *Langmuir* **2008**, *24*, 13258−13261.

(5) Iglic, A. *Advances in Planar Lipid Bilayers and Liposomes*; Elsevier: Oxford, U.K., 2011; Vol. *13*.

(6) Castellana, E. T.; Cremer, P. S. Solid Supported Lipid Bilayers: from Biophysical Studies to Sensor Design. *Surf. Sci. Rep.* **2006**, *61*, 429−444.

(7) Leonenko, Z. V.; Carnini, A.; Cramb, D. T. Supported Planar Bilayer Formation by Vesicle Fusion: the Interaction of Phospholipid Vesicles with Surfaces and the Effect of Gramicidin on Bilayer Properties Using Atomic Force Microscopy. *Biochim. Biophys. Acta* **2000**, *1509*, 131−147.
(8) Redondo-Morata, L.; Oncins, G.; Sanz, F. Force Spectroscopy Reveals the Effect of Different Ions in the Nanomechanical Behavior of Phospholipid Model Membranes: the Case of Potassium Cation. *Biophys. J.* **2012**, *102*, 66−74.
(9) Graff, A.; Winterhalter, M.; Meier, W. Nanoreactors from Polymer-Stabilized Liposomes. *Langmuir* **2001**, *17*, 919−923.
(10) Cremer, P. S.; Boxer, S. G. Formation and Spreading of Lipid Bilayers on Planar Glass Supports. *Biochemistry* **1996**, *35*, 14773−14781.
(11) Lipowsky, R.; Seifert, U. Adhesion of Vesicles and Membranes. *Mol. Cryst. Liq. Cryst.* **1991**, *202*, 17−25.
(12) Seifert, U. Configurations of Fluid Membranes and Vesicles. *Adv. Phys.* **1997**, *46*, 13−137.
(13) Wang, X.; Shindel, M. M.; Wang, S.-W.; Ragan, R. A Facile Approach for Assembling Lipid Bilayer Membranes on Template-Stripped Gold. *Langmuir* **2010**, *26*, 18239−18245.
(14) Naumann, R.; Schiller, S. M.; Giess, F.; Grohe, B.; Hartman, K. B.; Kärcher, I.; Köper, I.; Lübben, J.; Vasilev, K.; Knoll, W. Tethered Lipid Bilayers on Ultraflat Gold Surfaces. *Langmuir* **2003**, *19*, 5435−5443.
(15) Bordi, F.; Cametti, C.; Gliozzi, A. Impedance Measurements of Self-Assembled Lipid Bilayer Membranes on the Tip of an Electrode. *Bioelectrochemistry* **2002**, *57*, 39−46.
(16) Salamon, Z.; Wang, Y.; Tollin, G.; Macleod, H. A. Assembly and Molecular Organization of Self-Assembled Lipid Bilayers on Solid Substrates Monitored by Surface Plasmon Resonance Spectroscopy. *Biochim. Biophys. Acta* **1994**, *1195*, 267−275.
(17) Puu, G.; Gustafson, I. Planar Lipid Bilayers on Solid Supports from Liposomes-Factors of Importance for Kinetics and Stability. *Biochim. Biophys. Acta* **1997**, *1327*, 149−161.
(18) Wiegand, G.; Arribas-Layton, N.; Hillebrandt, H.; Sackmann, E.; Wagner, P. Electrical Properties of Supported Lipid Bilayer Membranes. *J. Phys. Chem. B* **2002**, *106*, 4245−4254.
(19) Gritsch, S.; Nollert, P.; Jähnig, F.; Sackmann, E. Impedance Spectroscopy of Porin and Gramicidin Pores Reconstituted into Supported Lipid Bilayers on Indium-Tin-Oxide Electrodes. *Langmuir* **1998**, *14*, 3118−3125.
(20) Popovich, N. D.; Wong, S.; Brian, K. H.; Yeom, Y. H.; Paine, D. C. Influence of Microstructure on the Electrochemical Performance of Tin-Doped Indium Oxide Film Electrodes. *Anal. Chem.* **2002**, *74*, 3127−3133.
(21) Yang, J.; Kleijn, J. M. Order in Phospholipid Langmuir-Blodgett Layers and the Effect of the Electrical Potential of the Substrate. *Biophys. J.* **1999**, *76*, 323−332.
(22) Devadoss, A. Cholesterol Oxidase Modified Microelectrodes for Detection of Cholesterol in the Plasma Membrane of Single Cells. Ph.D thesis, Case Western Reserve University, Cleveland, OH, 2006.
(23) Hillebrandt, H.; Wiegand, G.; Tanaka, M.; Sackmann, E. High Electric Resistance Polymer/Lipid Composite Films on Indium-Tin-Oxide Electrodes. *Langmuir* **1999**, *15*, 8451−8459.
(24) McBee, T. W.; Wang, L.; Ge, C.; Beam, B. M.; Moore, A. L.; Gust, D.; Moore, T,A; Armstrong, N. R.; Saavedra, S. S. Characterization of Proton Transport Across a Waveguide-Supported Lipid Bilayer. *J. Am. Chem. Soc.* **2006**, *128*, 2184−2185.
(25) Leonenko, Z. V.; Finot, E.; Ma, H.; Dahms, T. E. S.; Cramb, D. T. Investigation of Temperature-Induced Phase Transitions in DOPC and DPPC Phospholipid Bilayers Using Temperature-Controlled Scanning Force Microscopy. *Biophys. J.* **2004**, *86*, 3783−3793.
(26) Oncins, G.; Picas, L.; Hernández-Borrell, J.; Garcia-Manyes, S.; Sanz, F. Thermal Response of Langmuir-Blodgett Films of Dipalmitoylphosphatidylcholine Studied by Atomic Force Microscopy and Force Spectroscopy. *Biophys. J.* **2007**, *93*, 2713−2725.
(27) Garcia-Manyes, S.; Oncins, G.; Sanz, F. Effect of Temperature on the Nanomechanics of Lipid Bilayers Studied by Force Spectroscopy. *Biophys. J.* **2005**, *89*, 4261−4274.
(28) Swiezewska, E.; Dallner, G.; Andersson, B.; Ernster, L. Biosynthesis of Ubiquinone and Plastoquinone in the Endoplasmic Reticulum-Golgi Membranes of Spinach Leaves. *J. Biol. Chem.* **1993**, *268*, 1494−1499.
(29) Jono, R.; Yamashita, K. Two Different Lifetimes of Charge Separated States: a Porphyrin−Quinone System in Artificial Photosynthesis. *J. Phys. Chem. C* **2012**, *116*, 1445−1449.
(30) Nagata, T.; Kikuzawa, Y. An Approach Towards Artificial Quinone Pools by Use of Photo- and Redox-Active Dendritic Molecules. *Biochim. Biophys. Acta* **2007**, *1767*, 648−652.
(31) Gust, D.; Moore, T. A.; Moore, A. L. Solar Fuels via Artificial Photosynthesis. *Acc. Chem. Res.* **2009**, *42*, 1890−1898.
(32) Hoyo, J.; Guaus, E.; Torrent-Burgues, J.; Sanz, F. Electrochemical Behaviour of Mixed LB Films of Ubiquinone−DPPC. *J. Electroanal. Chem.* **2012**, *669*, 6−13.
(33) Hoyo, J.; Guaus, E.; Torrent-Burgues, J. Biomimetic Monolayer Films of Monogalactosyldiacylglycerol Incorporating Ubiquinone. *J. Colloid Interface Sci.* **2012**, *384*, 189−197.
(34) Florin, E. L.; Rief, M.; Lehmann, H.; Ludwig, M.; Dornmair, C.; Moy, V. T.; Gaub, H. E. Sensing Specific Molecular Interactions with the Atomic Force Microscope. *Biosens. Bioelectron.* **1995**, *10*, 895−901.
(35) Nussio, M. R.; Oncins, G.; Ridelis, I.; Szili, E.; Shapter, J. G.; Sanz, F.; Voelcker, N. H. Nanomechanical Characterization of Phospholipid Bilayer Islands on Flat and Porous Substrates: a Force Spectroscopy Study. *J. Phys. Chem. B* **2009**, *113*, 10339−10347.
(36) Mou, J.; Yang, J.; Huang, C.; Shao, Z. Alcohol Induces Interdigitated Domains in Unilamellar Phosphatidylcholine Bilayers. *Biochemistry* **1994**, *33*, 9981−9985.
(37) Leonenko, Z. V.; Cramb, D. T. Revisiting Lipid-General Anesthetic Interactions (I): Thinned Domain Formation In Supported Planar Bilayers Induced by Halothane and Ethanol. *Can. J. Chem.* **2004**, *82*, 1128−1138.
(38) Morandat, S.; El Kirat, K. Cytochrome c Provokes the Weakening of Zwitterionic Membranes as Measured by Force Spectroscopy. *Colloids Surf., B* **2011**, *82*, 111−117.
(39) Koubi, L.; Tarek, M.; Klein, M.; Scharf, D. Distribution of Halothane in a Dipalmitoylphosphatidylcholine Bilayer from Molecular Dynamics Calculations. *Biophys. J.* **2000**, *78*, 800−811.
(40) Jemiola-Rzeminska, M.; Kruk, J.; Skowronek, M.; Strzalka, K. Location of Ubiquinone Homologues in Liposome Membranes Studied by Fluorescence Anisotropy of Diphenyl-Hexatriene and Trimethylammonium-Diphenyl-Hexatriene. *Chem. Phys. Lipids* **1996**, *79*, 55−63.
(41) Butt, H. J.; Franz, V. Rupture of Molecular Thin Films Observed in Atomic Force Microscopy. I. Theory. *Phys. Rev. E: Stat., Nonlinear, Soft Matter Phys.* **2002**, *66*, 031601-1−031601-9.
(42) Loi, S.; Sun, G.; Franz, V.; Butt, H. J. Rupture of Molecular Thin Films Observed in Atomic Force Microscopy. II. Experiment. *Phys. Rev. E: Stat., Nonlinear, Soft Matter Phys.* **2002**, *66*, 031602-1−031602-7.
(43) Bilewicz, R.; Sek, S.; Zawisza, I. Electron Transport through Composite Monolayers. *Russ. J. Electrochem.* **2002**, *38*, 29−38.
(44) Zawisza, I.; Lachenwitzer, A.; Zamlynny, V.; Horswell, S. L.; Goddard, J. D.; Lipkowski, J. Electrochemical and Photon Polarization Modulation Infrared Reflection Absorption Spectroscopy Study of the Electric Field Driven Transformations of a Phospholipid Bilayer Supported at a Gold Electrode Surface. *Biophys. J.* **2003**, *85*, 4055−4075.
(45) Zawisza, I.; Bin, X.; Lipkowski, J. Spectroelectrochemical Studies of Bilayers of Phospholipids in Gel and in Liquid State on Au(111) Electrode Surface. *Bioelectrochemistry* **2004**, *63*, 137−147.
(46) Lipkowski, J. Building Biomimetic Membrane at a Gold Electrode Surface. *Phys. Chem. Chem. Phys.* **2010**, *12*, 13874−13887.
(47) Daskalakis, N. N.; Müller, A.; Evans, S. D.; Jeuken, L. J. C. Driving Bioenergetic Processes with Electrodes. *Soft Matter* **2011**, *7*, 49−52.

(48) Bard, A. J.; Falkner, L. R. *Electrochemical Methods. Fundamentals and Applications*; John Wiley & Sons: New York, 2001.
(49) Shiba, H.; Maeda, K.; Ichieda, N.; Kasuno, M.; Yoshida, Y.; Shirai, O.; Kihara, S. Voltammetric Study on the Electron Transport through a Bilayer Lipidmembrane Containing Neutral or Ionic Redox Molecules. *J. Electroanal. Chem.* **2003**, *556*, 1−11.
(50) Demel, R. A.; Geurts Van Kessel, W. S. M.; Zwaal, R. F. A.; Roelofsen, B.; Van Deenen, L. L. M. Relation between Various Phospholipase Actions on Human Red Cell Membranes and the Interfacial Phospholipid Pressure in Monolayers. *Biochim. Biophys. Acta* **1975**, *406*, 97−107.

dx.doi.org/10.1021/jp4004517 | *J. Phys. Chem. B* XXXX, XXX, XXX−XXX